ARTICLES

Liquid Crystal Phase Transitions in Systems of Colloidal Platelets with Bimodal Shape Distribution

A. A. Verhoeff,*,† H. H. Wensink,‡ M. Vis,† G. Jackson,‡ and H. N. W. Lekkerkerker†

Van't Hoff Laboratory for Physical and Colloid Chemistry, Debye Institute, Utrecht University, Padualaan 8, 3584 CH Utrecht, The Netherlands, and Department of Chemical Engineering, Imperial College London, South Kensington Campus, London SW7 2AZ, United Kingdom

Received: March 30, 2009; Revised Manuscript Received: July 17, 2009

We have studied a system of polydisperse, charged colloidal gibbsite platelets with a bimodal distribution in the particle aspect ratio. We observe a density inversion of the coexisting isotropic and nematic phases as well as a three-phase equilibrium involving a lower density nematic phase, an isotropic phase of intermediate density, and a higher density columnar phase. To relate these phenomena to the bimodality of the shape distribution, we have calculated the liquid crystal phase behavior of binary mixtures of thick and thin hard platelets for various thickness ratios. The predictions are based on the Onsager−Parsons theory for the isotropic−nematic (I−N) transition combined with a modified Lennard-Jones−Devonshire cell theory for the columnar (C) state. For sufficiently large thickness ratios, the phase diagram features an I−N density inversion and triphasic I−N−C equilibrium, in agreement with experiment. The density inversion can be attributed to a marked shape fractionation among the coexisting phases with the thick species accumulating in the isotropic phase. At high concentrations, the theory predicts a coexistence between two columnar phases with distinctly different concentrations. In experiment, however, the demixing transition is pre-empted by a transition to a kinetically arrested, glassy state with structural features resembling a columnar phase.

I. Introduction

The phase behavior of bidisperse colloidal systems incorporates many intriguing phenomena such as the formation of stable superstructures and phase equilibria involving multiple phases. For example, mixtures of spheres with a diameter ratio of around 0.5 are known to form AB_2 and AB_{13} binary crystals, as first observed in natural opals[1,2] and reproduced in suspensions of latex particles[3,4] and colloidal hard spheres.[5−7] Mixtures of long and short rod-like colloids exhibit a demixing of the nematic phase which leads to a coexistence of two nematic phases with different compositions including a triphasic isotropic−nematic−nematic equilibrium, as observed experimentally[8,9] and confirmed by theory.[10] A similar behavior has been observed recently in binary mixtures of thin and thick hard rods with equal length,[11] as originally predicted with an Onsager−Parsons description.[12]

In contrast to rods, the phase behavior of plate-shaped colloids has only been explored over the past decade.[13−18] A remarkable feature of some of these systems is that the formation of a partially crystalline columnar phase is not suppressed by the considerable spread in particle size,[15] as is the case with crystalline and smectic order in polydisperse systems of spheres[19] and rods.[20] Moreover, a large spread in the plate thickness may give rise to a so-called isotropic−nematic *density inversion*, in which the isotropic phase becomes denser than the coexisting nematic. This phenomenon originates from a pronounced fractionation in the thickness of the particles among the coexisting phases with the thick species accumulating in the isotropic phase and the thin ones in the nematic phase. Although the nematic phase has a higher particle concentration than the isotropic phase, its mass density falls below that of the isotropic phase due to a high fraction of thin platelets with a lower particle mass. This phenomenon has been observed in a polydisperse system of *sterically* stabilized gibbsite platelets[21] and analyzed with a simple theory based on Onsager's second-virial theory extended to binary mixtures.[22] A similar density inversion can be predicted from fundamental measure theory based on the Zwanzig model for binary hard platelets.[23]

In this Article, we report our findings on a system of *charged* gibbsite platelets, which forms a remarkable three-phase equilibrium, involving a low-density nematic phase, an isotropic phase of intermediate density, and a dense columnar phase. A size analysis using atomic force microscopy (AFM) reveals that the distribution of the aspect ratio, defined as the plate thickness-to-diameter ratio, is characterized by a distinct bimodal shape. In an analogous fashion to the sterically stabilized system,[21] the charged plate system exhibits a density inversion of the isotropic and nematic phases induced by a strong fractionation effect with respect to the aspect ratio. The fractionation scenario is corroborated by the size distributions measured in the coexisting phases, which demonstrate that the isotropic phase is rich in thick platelets, while the corresponding nematic phase consists mainly of thin platelets corresponding to a small aspect ratio.

* To whom correspondence should be addressed. E-mail: a.a.verhoeff@uu.nl.
† Utrecht University.
‡ Imperial College London.

10.1021/jp902858k CCC: $40.75
Published on Web 09/17/2009

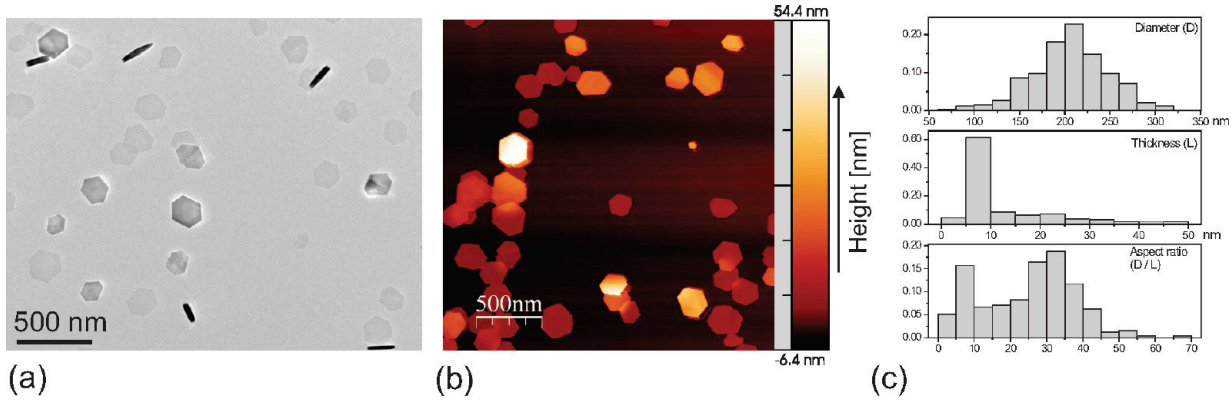

Figure 1. (a) Transmission electron micrograph and (b) atomic force micrograph of the gibbsite platelets. (c) Histograms of the diameter, thickness, and aspect ratio *D*/*L* of the platelets, determined with atomic force microscopy.

A theoretical underpinning of the observed effects is provided by calculating the phase diagram of a binary mixture of thin and thick platelets for various thickness ratios. This is done by combining the Onsager−Parsons theory for the isotropic to nematic transition with a modified Lennard-Jones−Devonshire cell theory for the columnar state.[24] For a sufficiently large ratio of the particle thickness, the I−N density inversion and triphasic isotropic−nematic−columnar coexistence can both be satisfactorily reproduced. Moreover, at high particle concentrations, our theory predicts a demixing of the columnar phase into a fraction containing predominantly thin species and a "mixed" fraction with equal portions of thin and thick platelets. This demixing could not be observed in the experimental system due to the formation of a dynamically arrested glassy state at high particle concentrations.

II. Materials and Methods

Gibbsite platelets were synthesized by hydrothermal treatment of aluminum alkoxides,[25] and subsequently treated with aluminum chlorohydrate to increase particle stability. The enhanced stability is associated with the presence of aluminum polycations which are formed upon addition of the aluminum salt. At pH $\approx$ 4, the cations hydrolyze and adsorb on the surface of the gibbsite particles. This gives rise to a steep repulsive particle interaction which prevents the platelets from aggregating.[26]

The gibbsite platelets were analyzed with transmission electron microscopy (TEM) using a Tecnai 10 microscope (FEI Company) and atomic force microscopy (AFM) utilizing a multimode scanning probe microscope (Digital Instruments). AFM measurements were performed in tapping mode with a standard TESP silicon tip. Samples were prepared by dilution of the gibbsite dispersion with a 1:1 water−ethanol mixture. The diluted suspension was subsequently spread onto carbon-coated copper grids (TEM measurements) or freshly cleaved mica (AFM measurements). To obtain the distributions of the particle dimensions, the diameter, thickness, and aspect ratio of 200−270 particles were measured.

The gibbsite platelets had a well-defined hexagonal shape (see the micrographs in Figure 1a and b), with an average diameter of 207 nm with a standard deviation in the average σ_D of 35% and an average thickness of 8.2 nm with a σ_L of 46%. The diameter of the platelets had a rather broad, symmetrical distribution, while the thickness was strongly peaked with a long tail toward the thicker particles (see Figure 1c). The aspect ratio, however, was bimodal, with a relatively narrow distribution of thick species and a much wider spread of thin ones.

The gibbsite dispersion was concentrated via centrifugation and redispersion with 10^{-2} M NaCl to the concentration where phase separation was just hindered by kinetic arrest. Samples of decreasing concentration were prepared upon dilution and stored in 50 × 4 × 0.2 mm^3 sized glass capillaries (VitroCom), which were flame-sealed and subsequently glued to avoid evaporation of the solvent. The suspensions were left to phase separate and equilibrate at room temperature for 2 weeks.

The phase behavior of the system was studied on a macroscopic scale by placing the capillaries between crossed polarizers, where they were photographed with a Nikon Coolpix 995 digital camera. The samples were examined in more detail using a Nikon LV100 Pol polarizing microscope with 10× and 20× Nikon ELWD Plan Fluor objectives, and equipped with a QImaging MicroPublisher 5 megapixel CCD camera. Bragg reflections were observed with the polarizing microscope while the sample was illuminated with a cold light source (Dolan Jenner, model 190).

III. Phase Behavior Experiments

In Figure 2a, we show a concentration series of the charge stabilized gibbsite platelets. Upon increasing the particle concentration, the system enters the isotropic−nematic biphasic regime, with a nematic phase at the bottom and an isotropic phase at the top of the capillary, separated by a sharp interface. Further increasing the particle concentration leads to the onset of a density inversion, where the isotropic phase starts to become denser than the nematic phase. Around the inversion point, the I−N interface shows a regular pattern of fingers reminiscent of a Rayleigh−Taylor instability (see the second capillary of Figure 2a and the enlarged view in part b).[27] At higher concentrations, the inverted state is reached with a nematic top phase and an isotropic bottom phase, separated by a sharp interface. Upon subsequent densification, the system enters a triphasic region, where the isotropic phase is located between a nematic upper phase and a columnar bottom phase, all separated by sharp interfaces. The columnar bottom phase is also characterized by bright Bragg reflections (see Figure 2c), which originate from the two-dimensional hexagonal arrangement of the columnar stacks of platelets. The color associated with the Bragg reflections ranges from green to red, which corresponds to an average intercolumnar distance of about ~250 nm. When the particle concentration is further increased, the isotropic phase disappears, leaving an upper nematic phase in coexistence with a lower columnar phase. Finally, at very high concentrations, an arrested state is reached which no longer undergoes

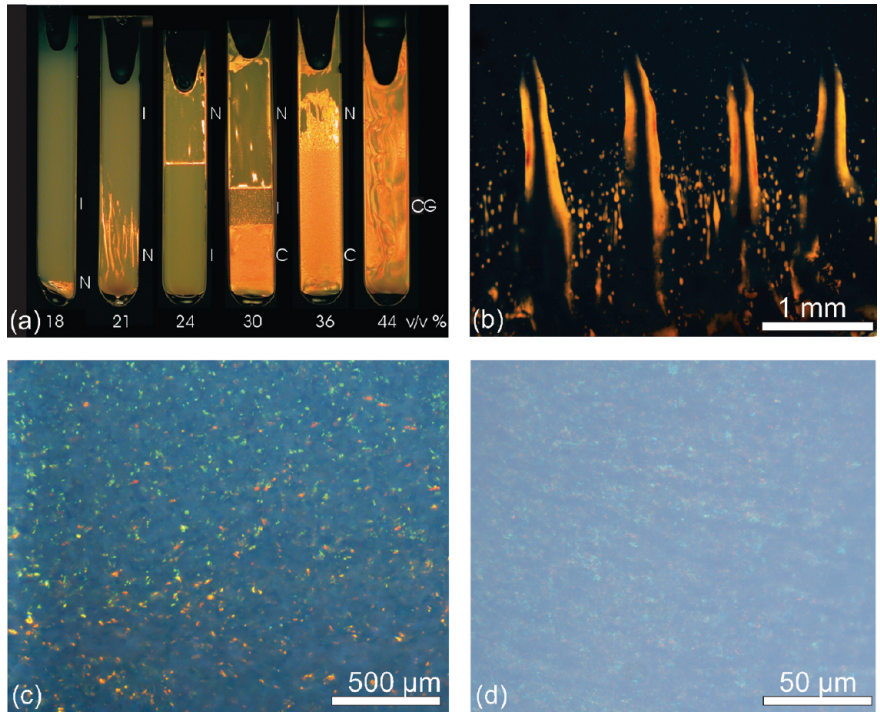

Figure 2. (a) Concentration series of suspensions of charged gibbsite platelets. A sequence of phase equilibria is observed, ranging from biphasic isotropic−nematic (I−N), inverted biphasic isotropic−nematic (I−N), triphasic isotropic−nematic−columnar (I−N−C), biphasic nematic−columnar (N−C), to a columnar glass (CG). (b) Regular fingering pattern in an isotropic−nematic sample at a density of 20 v/v %, close to the inversion point. Bragg reflections in the columnar phase (c) and in the dynamically arrested columnar glass (d).

macroscopic phase separation. Birefringent patterns are clearly visible and persist over a long time. These correspond to "frozen-in" regions of particle alignment caused by the shear forces during the filling of the capillary. The sample also shows Bragg reflections originating from small grains with a domain size of about 5 μm, as depicted in Figure 2d. This indicates that, despite the high packing fraction, the platelets still have enough free volume to locally self-assemble into columnar arrangements.

The capillary containing the inverted isotropic−nematic phase equilibrium was further investigated by splitting the capillary and analyzing the two coexisting phases separately with AFM. In Figure 3, we depict the sample between crossed polarizers together with AFM images of the gibbsite platelets in both phases. The measured diameter, thickness, and (inverse) aspect ratio distributions of the platelets in the isotropic and nematic phases are presented in Figure 4. Although the diameter distribution is virtually the same in both phases, the thickness distributions are significantly different, with the isotropic phase markedly enriched in thick platelets. The most distinct difference can be inferred from the histograms showing the aspect ratio distribution in both phases. From this, it is evident that the nematic phase is characterized by a unimodal distribution of thin platelets (large D/L), whereas the isotropic phase possesses a bimodal shape distribution with a significant fraction of thick species (small D/L).

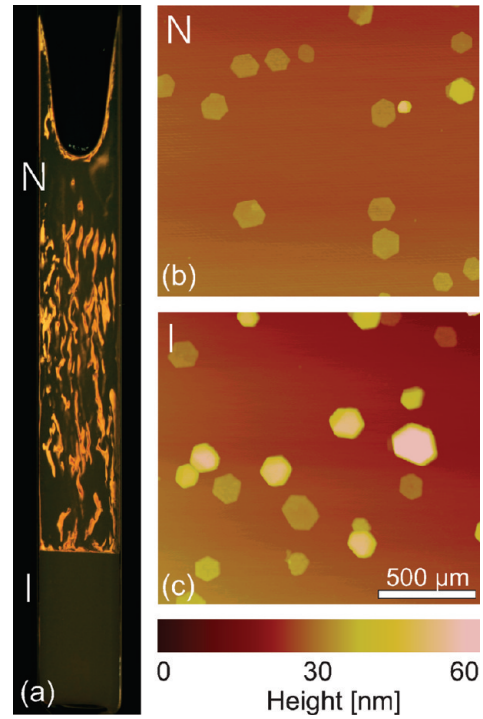

Figure 3. (a) Image of a gibbsite suspension with isotropic−nematic density inversion, taken between crossed polarizers. AFM images of gibbsite platelets sampled from the nematic (b) and isotropic (c) phase.

IV. Onsager−Parsons Theory for the Isotropic−Nematic Transition

A simple theory is now employed to describe the main features of the experimental system. For the present system of charged platelets, a theory would be required based on a hard-core model supplemented with a suitable electrostatic potential. Unfortunately, the effective (screened) pair potential between two uniformly charged platelets resulting from the Poisson−Boltzmann theory is not known in analytical form[28] and multipole expansions—aimed at providing an analytical approximation valid at large plate separations—are questionable at high particle densities (in particular in the nematic and columnar phases). Headway can be made by restricting the plate

orientations to the three Cartesian axes. Within the so-called Zwanzig approximation, a tractable density functional theory can be formulated which allows one to scrutinize the effect of charge on the structure and phase behavior of colloidal platelets.[29] Alternatively, interaction site models, based on a discretization of the surface charge into Yukawa sites compacted onto a circular disk-shaped array, can be analyzed with integral equation theory to elucidate the pair correlation functions of charged platelets at low to moderate densities.[30]

The scope of our current paper is to keep the theory as tractable as possible while maintaining the essential physics of the problem. Therefore, we will build on the simple but physically plausible idea that the main effect of the double layers is to alter the effective shape of the platelets, such that the effective thickness by which the platelets interact is enhanced. The use of an effective hard particle is merited by the fact that the electric double layers surrounding the platelets are rather tight.[42]

Let us consider a binary mixture of $N = N_1 + N_2$ hard cylinders with two different lengths, L_1 and L_2, and common diameter $D = D_1 = D_2$ in a macroscopic volume V. For the plate-like cylinders we consider here, the inverse aspect ratio L_i/D ($i = 1,2$) is much smaller than unity. Henceforth, we shall assign the label "2" to the thickest particles. The overall concentration of the system is expressed in dimensionless form via $c = ND^3/V$. Following ref 22, the Onsager−Parsons Helmholtz free energy of such a mixture at a given c and mole fraction $x_i = N_i/N$ is given by

$$\frac{\beta F}{N} = (\ln \tilde{\mathcal{V}} c - 1) + \sum_{i=1,2} x_i\{\ln x_i + \langle \ln 4\pi f_i\rangle_i\} + \frac{cG_P(\phi)}{2}\sum_i \sum_j x_i x_j \langle\langle \tilde{V}^{ij}_{excl}(\gamma)\rangle\rangle_{ij} \quad (1)$$

where $\beta^{-1} = k_B T$ is the thermal energy and $\tilde{\mathcal{V}} = \prod_i \mathcal{V}_i^{x_i}/D^3$, with $\mathcal{V}_i$ being the thermal volume of species i (including contributions arising from the rotational momenta of the platelet). The brackets $\langle(\bullet)\rangle_i = \int d\Omega f_i(\Omega)(\bullet)$ denote an orientational average according to some unknown orientational distribution function f_i, normalized via $\int d\Omega f_i(\Omega) = 1$. Several entropic contributions can be distinguished in eq 1. The first three are *exact* and denote the ideal translational, mixing, and orientational entropy, respectively. The last term represents the excess translational or packing entropy which accounts for the particle correlations on the approximate second-virial level by considering pair interactions only. The key quantity here is the excluded volume V^{ij}_{excl} between two plate-like cylinders of type i and j at fixed interparticle angle γ:[31]

$$\tilde{V}^{ij}_{excl}(\gamma) = \frac{V^{ij}_{excl}(\gamma)}{D^3} = \frac{\pi}{2}|\sin\gamma| + \left(\frac{L_i}{D} + \frac{L_j}{D}\right)\left(\frac{\pi}{4} + E(\sin\gamma) + \frac{\pi}{4}\cos\gamma\right) + 2\frac{L_i L_j}{D^2}|\sin\gamma| \quad (2)$$

with $E(x)$ being the complete elliptic integral of the second kind.

Although the structure of eq 1 is similar to the classic Onsager second-virial free energy, higher order virial terms are incorporated approximately through a density rescaling according to Parsons' recipe[32−34] as extended to mixtures (see ref 35 for a recent review of the use of the Onsager−Parsons free energy to describe mixtures of hard particles). This involves a rescaled density cG_P where the factor $G_P = (1 - 3\phi/4)/(1 - \phi)^2$ depends on the total plate volume fraction $\phi = c\sum_i x_i(\pi L_i/4D)$. Note that G_P approaches unity in the low-density limit $\phi \to 0$ in which case the original second-virial theory is recovered, as required.

One must then specify the orientational averaging. By definition, all orientations are equally probable in the isotropic (I) phase and $f_i = 1/4\pi$. The orientational contributions then simply become

$$\langle \ln 4\pi f_i\rangle_i \equiv 0 \qquad \text{(I)} \quad (3)$$

Using the isotropic averages $\langle\langle \sin\gamma\rangle\rangle = \pi/4$, $\langle\langle E(\sin\gamma)\rangle\rangle = \pi^2/8$ and $\langle\langle \cos\gamma\rangle\rangle = 1/2$, we obtain for the excluded volume contribution

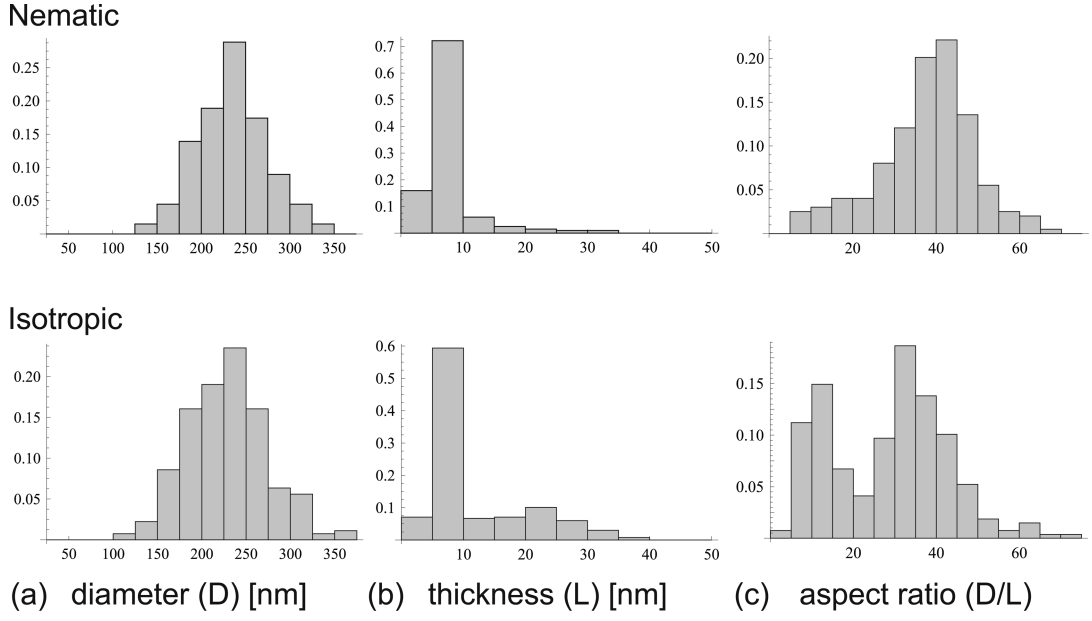

Figure 4. Histograms of the platelet diameter (a), thickness (b), and aspect ratio (c) sampled from the nematic and isotropic phase of a sample with isotropic−nematic density inversion (see Figure 3), determined with AFM.

$$\langle\langle \tilde{V}^{ij}_{\mathrm{excl}}(\gamma)\rangle\rangle = \frac{\pi^2}{8} + \left(\frac{L_i}{D} + \frac{L_j}{D}\right)\left(\frac{3\pi}{8} + \frac{\pi^2}{8}\right) + \frac{L_i L_j}{D^2}\frac{\pi}{2} \tag{4}$$

In the nematic (N) phase, the particles are expected to be oriented along a common nematic director. For strongly ordered states, it is expedient to adopt a Gaussian trial function to describe the orientational probability density.[36] For a uniaxial nematic phase, the Gaussian trial function takes on the following form:

$$f_i(\theta) \equiv \begin{cases} \dfrac{\alpha_i}{4\pi}\exp\left[-\dfrac{1}{2}\alpha_i\theta^2\right] & \text{if } 0 \le \theta \le \dfrac{\pi}{2} \\ \dfrac{\alpha_i}{4\pi}\exp\left[-\dfrac{1}{2}\alpha_i(\pi-\theta)^2\right] & \text{if } \dfrac{\pi}{2} < \theta \le \pi \end{cases} \tag{5}$$

with θ being the polar angle between the plate normal and the nematic director and $\alpha_i \gg 1$ a variational parameter. With the use of the Gaussian trial function, the orientational averages in the free energy can be rendered analytically tractable by performing asymptotic expansions for large α_i and retaining the leading order terms. The result for the orientational entropy is

$$\langle \ln 4\pi f_i\rangle_i \sim \ln \alpha_i - 1 \qquad \text{(N)} \tag{6}$$

For small angles γ, the orientationally averaged excluded volume can be expanded as follows:

$$\langle\langle \tilde{V}^{ij}_{\mathrm{excl}}(\gamma)\rangle\rangle_{ij} = \pi\left(\frac{L_i}{D} + \frac{L_j}{D}\right) + \left(\frac{\pi}{2} + \frac{2L_iL_j}{D^2}\right)\langle\langle\gamma\rangle\rangle_{ij} + \mathcal{O}\langle\langle\gamma^2\rangle\rangle_{ij} \tag{7}$$

Within the Gaussian approximation, the double orientational average of γ is given by[37]

$$\langle\langle\gamma\rangle\rangle_{ij} \sim \left(\frac{\pi}{2}\right)^{1/2}\left(\frac{1}{\alpha_i} + \frac{1}{\alpha_j}\right)^{1/2} \tag{8}$$

up to leading order in α_i, while $\langle\langle\gamma^2\rangle\rangle_{ij} \sim \mathcal{O}(\alpha i/j - 1)$ generates the next-leading order terms which we will neglect here. If we further assume the inverse plate aspect ratio to be sufficiently small so that all contributions of order L_iL_j/D^2 are of negligible importance, the resulting double orientationally averaged excluded volume in the nematic phase can be approximated as

$$\langle\langle \tilde{V}^{ij}_{\mathrm{excl}}(\gamma)\rangle\rangle_{ij} \sim \pi\left(\frac{L_i}{D} + \frac{L_j}{D}\right) + \left(\frac{\pi}{2}\right)^{3/2}\left(\frac{1}{\alpha_i} + \frac{1}{\alpha_j}\right)^{1/2} \tag{9}$$

which has the important advantage that the Gaussian variational parameters are now fully *decoupled* from the thickness. Inserting this result together with eq 6 into the free energy and minimizing with respect to α_i yields a simple quadratic concentration dependence for the equilibrium value of α_i:

$$\alpha_i \sim \frac{4}{\pi}(cG_{\mathrm{P}})^2, \qquad i = 1, 2 \tag{10}$$

which is the same result as that for the monodisperse case.[38] Since there are no explicit minimization equations for α_i to be solved, the nematic free energy for the mixtures is entirely algebraic. Phase equilibria between isotropic and nematic states are found in the usual numerical way by imposing equality of chemical potentials μ_i of each component i and pressure P. These quantities are obtained from the free energy using the standard thermodynamic derivatives, $P = -(\partial F/\partial V)_{NVT}$ and $\mu_i = (\partial F/\partial N_i)_{N_jVT}$.

V. Cell Theory for the Columnar Phase

To describe the thermodynamical properties of a columnar phase, we use an extended cell theory as proposed in ref 24. In this approach, the structure of a columnar phase is envisioned in terms of columns ordered along a perfect lattice in two lateral dimensions with a strictly one-dimensional fluid behavior of the constituents in the remaining direction along the columns. As for the latter, the canonical partition function of a binary mixture of *parallel* platelets with thicknesses L_1 and L_2 (and equal diameter D) with their center of mass moving along the plate normal on a line of length l is formally given by

$$Q_{\mathrm{fluid}}(N_1, N_2, l, T) = \frac{[l - (N_1L_1 + N_2L_2)]^N}{\Lambda_1^{N_1}\Lambda_2^{N_2}N_1!N_2!} \tag{11}$$

with Λ_i being the thermal de Broglie wavelength of the respective particle species. Next, we allow the plate orientation vectors to deviate slightly from the column direction. At high packing fractions, the rotational freedom of each platelet is assumed to be asymptotically small and the configurational integral above may be approximated as follows

$$Q_{\mathrm{fluid}}(N_1, N_2, l, T) \approx \frac{Q_1^{\mathrm{or}}Q_2^{\mathrm{or}}}{(\mathcal{V}_1^{\mathrm{l}})^{N_1}(\mathcal{V}_2^{\mathrm{l}})^{N_2}N_1!N_2!} \times [l - (N_1\langle L_1^{\mathrm{eff}}\rangle_1 + N_2\langle L_2^{\mathrm{eff}}\rangle_2)]^N \tag{12}$$

where $\mathcal{V}_i^{\mathrm{l}}$ represents the 1D thermal volume of species i including contributions arising from the (3D) rotational momenta of the platelet. Furthermore, $Q_i^{\mathrm{or}} = \exp[-N_i\langle\ln 4\pi f_i\rangle_i]$ is an orientational partition function depending on the orientational probability density distribution f_i of platelets of type i. In the *mean-field* description implied by eq 12, there is no coupling between the orientational degrees of freedom of the platelets. The rotation of the platelets becomes manifest in an *effective entropic thickness*, defined as

$$\langle L_i^{\mathrm{eff}}\rangle_i = L_i\left\{1 + \frac{1}{2}\frac{D}{L_i}\int \mathrm{d}(\cos\theta)|\theta|f_i(\theta) + \ldots\right\} \tag{13}$$

up to leading order in the polar angle θ which describes the deviation of the plate normal from the direction of the column. The prefactor of "1/2" in eq 13 has been included to correct in part for the azimuthal rotational freedom and captures the effect that the excluded length between two platelets at fixed polar angles becomes minimal when the azimuthal orientations are the same. The free energy of the 1D fluid then follows from $\beta F = -\ln Q$:

$$\frac{\beta F_{\text{fluid}}}{N} \sim (\ln \tilde{\mathcal{V}}\rho_0 - 1) + \sum_{i=1,2} x_i\{\ln x_i + \langle \ln 4\pi f_i\rangle_i\} - \ln[1 - \rho_0 \sum_i x_i q_i \langle \tilde{L}_i^{\text{eff}}\rangle_i] \quad (14)$$

where $\tilde{\mathcal{V}}^1 = \prod_i (\mathcal{V}^1)^{x_i}/L_0$. Furthermore, $\rho_0 = NL_0/l$ (with L_0 being some reference thickness), $q_i = L_i/L_0$, and $\tilde{L}_i^{\text{eff}} = L_i^{\text{eff}}/L_i$. The equilibrium forms for the distributions $f_i(\theta)$ are found by a formal minimization of the free energy while constraining them to be normalized. The corresponding stationarity condition is

$$\frac{\delta}{\delta f_i}\left(\frac{\beta F_{\text{fluid}}}{N} - \lambda_i \int \mathrm{d}(\cos\theta) f_i(\theta)\right) = 0 \quad (15)$$

with λ_i being a Lagrange multiplier. The solutions can be obtained in closed form and turn out to be of simple exponential form:

$$f_i(\theta) = \frac{\xi_i^2}{4\pi} \exp[-\xi_i|\theta|] \quad (16)$$

with

$$\xi_i = \left(\frac{3}{2}\frac{D}{L_i}\right)\frac{\rho_0 q_i}{1 - \rho_0(x_1 q_1 + x_2 q_2)} \quad (17)$$

The orientational averaging is now easily carried out, and the expressions for the orientational entropy and entropic thickness are given by

$$\langle \ln 4\pi f_i\rangle_i = 2 \ln \xi_i - 2$$
$$\langle \bar{L}_i^{\text{eff}}\rangle_i = 1 + \left(\frac{D}{L_i}\right)\frac{1}{\xi_i} \quad (18)$$

We now turn to the free energy associated with the positional order along the lateral directions of the columnar liquid crystal. A formal way to proceed is to map the system onto an ensemble of N disks ordered on a 2D lattice. Near close packing, the configurational integral of the system is well approximated by the Lennard-Jones and Devonshire cell model[39,40] so that we may write

$$Q_{\text{cell}}(N) = \Lambda^{-2N} \int \mathrm{d}\mathbf{r}^N \exp[-\beta U(\mathbf{r}^N)] \approx \left(\Lambda^{-2} \int \mathrm{d}^2\mathbf{r} \exp\left[-\frac{\beta}{2} u_{\text{cell}}^{\text{nn}}(\mathbf{r})\right]\right)^N \quad (19)$$

and recall that $N = N_1 + N_2$. Within the framework of the cell model, particles are considered to be localized in "cells" centered on the sites of a fully occupied lattice (of some prescribed symmetry). Each particle experiences a potential energy $u_{\text{cell}}^{\text{nn}}(\mathbf{r})$ generated by its nearest neighbors. In the simplest version, the theory presupposes that each cell contains one particle moving *independently* from its neighbors. For hard interactions, the second phase space integral is simply the cell *free area* available to each particle. If we assume the nearest neighbors to form a perfect hexagonal cage, the free area is given by $A_{\text{free}} = \sqrt{3}(\Delta_c - D)^2/2$, with Δ_c being the nearest neighbor distance. The configurational integral then becomes

$$Q_{\text{cell}}(N) \approx (\Lambda^{-2} A_{\text{free}})^N \sim (1 - \bar{\Delta}_c^{-1})^{2N} \quad (20)$$

in terms of the dimensionless lateral spacing $\bar{\Delta}_c = \Delta_c/D$. Applying the condition of single occupancy (i.e., one array of platelets per column), we can use $\bar{\Delta}_c$ to relate the *overall* particle volume fraction $\phi_0 = (\pi/4)NL_0D^2/V$ to the overall linear density ρ_0 via

$$\phi_0^* \bar{\Delta}_c^2 = \rho_0 \quad (21)$$

where $\phi_0^* = \phi_0/\phi_{cp}$ is a reduced variable in terms of $\phi_{cp} = \pi/(2\sqrt{3}) \approx 0.907$, the volume fraction at close packing. The total free energy of the columnar state is now obtained by combining the fluid and cell contributions

$$\frac{\beta F}{N} \sim (\ln \tilde{\mathcal{V}} - 1) + \sum_i x_i\left\{\ln x_i + 2 \ln\left(\frac{3}{2}\frac{D}{L_i}\frac{\phi_0^* q_i}{\bar{\Delta}_c^{-2} - \phi^*}\right)\right\} - \ln\left(\frac{1 - \phi^* \bar{\Delta}_c^2}{3}\right) - 2 \ln(1 - \bar{\Delta}_c^{-1}) \quad (22)$$

with $\tilde{\mathcal{V}}$ being the 3D thermal volume (cf. eq 1) and

$$\phi^* = \phi_0^*(x_1 q_1 + x_2 q_2) \quad (23)$$

is the *total* reduced packing fraction of the system. The final step is to minimize the total free energy with respect to $\bar{\Delta}_c$. The stationarity condition $\partial F/\partial \bar{\Delta}_c = 0$ yields a third-order polynomial whose physical solution reads

$$\bar{\Delta}_c = \frac{-3^{1/3} 4\phi^* + 2^{1/3} K^{2/3}}{6^{2/3} \phi^* K^{1/3}} \quad (24)$$

with

$$K = 27(\phi^*)^2 + [3(\phi^*)^3(32 + 243\phi^*)]^{1/2} \quad (25)$$

which is the same result as one would get for the monodisperse case, since the lateral spacing does not depend explicitly on the composition of the mixture (but only implicitly via eq 23). A more manageable expression for $\bar{\Delta}_c$ can be obtained by performing a Taylor expansion around the close packing limit, using $(1 - \phi^*)$ as a smallness parameter:

$$\bar{\Delta}_c = 1 + \frac{1}{5}(1 - \phi^*) + \frac{12}{125}(1 - \phi^*)^2 + \frac{178}{3125}(1 - \phi^*)^3 + \ldots \quad (26)$$

This cubic expression provides an excellent description of the exact result with a discrepancy of less than 0.1% throughout the entire range of relevant densities ($0.5 < \phi^* < 1$). As in the case of the Onsager−Parsons free energy of the nematic state, our treatment is entirely algebraic and no explicit minimization conditions need to be solved numerically along with the

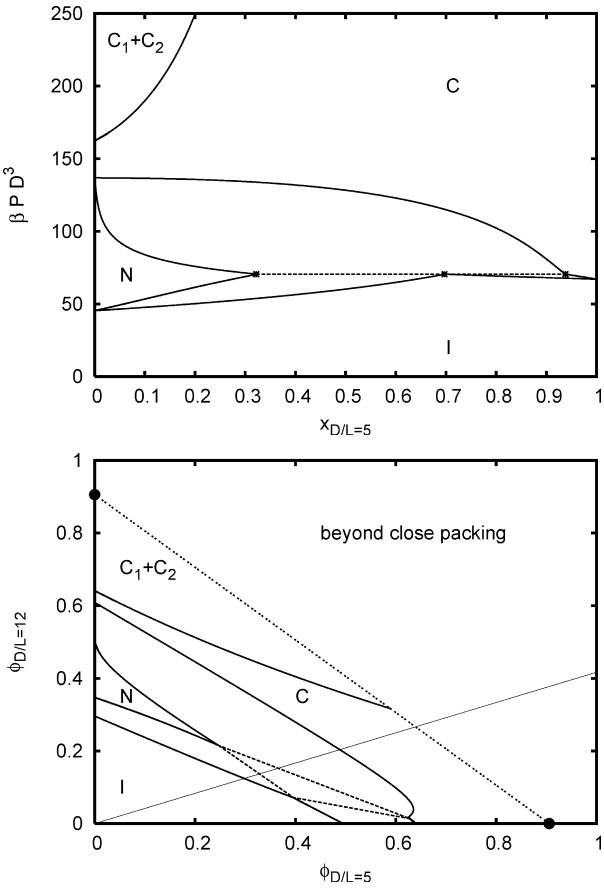

Figure 5. Phase diagram of a binary mixture of platelets with $D/L_1 = 12$ and $D/L_2 = 5$ ($L_2/L_1 = 2.4$) in the pressure−composition plane (top) and the density−density plane (bottom). Triphasic equilibria are indicated by dashed lines which form a triangle in the density−density representation. The thin continuous line running from the origin represents an equimolar dilution line ($x_1 = x_2 = 0.5$). The line connecting the filled circles denotes the bound of the unphysical region beyond close packing.

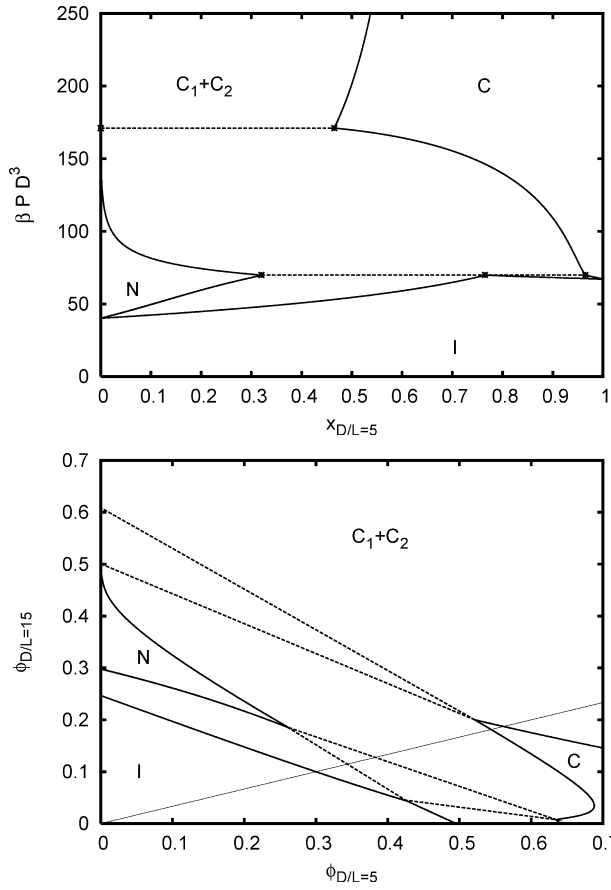

Figure 6. As Figure 5 for the binary mixture with $D/L_1 = 15$ and $D/L_2 = 5$ ($L_2/L_1 = 3$).

coexistence conditions. The latter can be established in the usual way from the pressure and chemical potentials associated with eq 22.

We now have all the ingredients needed for the calculation of the phase diagram, which are constructed for mixtures of platelets with distinctly different anisotropies. More precisely, we will consider binary systems consisting of thin platelets (which exhibit the full isotropic−nematic−columnar (I−N−C) phase sequence in its pure state), mixed with thick ones (which only have an isotropic−columnar (I−C) transition).[43] To best match the experimental systems, we shall fix the aspect ratio of the thick species to $D/L = 5$ and vary that of the thin species within the interval $10 < D/L < 15$. Taking into account the electrostatic screening effect induced by the electric double layers, these numbers provide reasonable estimates for the *effective* aspect ratios associated with the two peaks in the histograms of the "real" aspect ratio of the system shown in Figure 1c.

VI. Results and Discussion

With the theoretical approach described in the previous sections, the phase behavior of the polydiperse charged plate system can be reproduced qualitatively. Representative examples of the theoretical predictions of the phase diagram are shown in Figures 5 and 6. In both cases, there is a marked triple I−N−C equilibrium extending over a considerable range of overall compositions. Since the relative proportion of thick and thin platelets is fixed in the experimental system, we can draw a dilution line in Figure 5 which samples a sequence of phase equilibria observed in the experiments. These range from a biphasic isotropic−nematic, through a triphasic isotropic−nematic−columnar, to a nematic−columnar biphasic equilibrium found at high concentrations.

A density inversion occurs upon traversing the isotropic−nematic coexistence region, as illustrated in Figure 7. As alluded to earlier, this observation stems from the pronounced fractionation among the coexisting phases with a high proportion of thin species concentrated in the nematic phase.[22] This behavior becomes manifest in the pressure−composition representations of the phase diagram where the mole fraction of thick species is found to be systematically larger in the isotropic phase, in agreement with the histograms depicted in Figure 4. We note that, experimentally, the density inversion appears to be driven by a fractionation in shape (i.e., aspect ratio) rather than the plate thickness alone.

In the region of the density inversion, the interface exhibits a regular pattern of fingers with a spacing of about 1 mm. Such a pattern is reminiscent of the Rayleigh−Taylor instability,[27,41] which occurs when the density in the upper phase is higher than that in the lower phase. Since the density difference between both phases is very small near the inversion point, small density gradients induced by gravity may already give rise to such an instability. The observation of a pattern with a wavelength of about 1 mm is in agreement

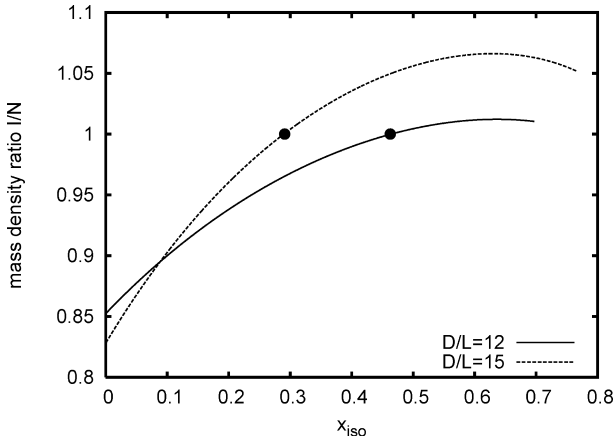

Figure 7. Mass density ratio $\sum_i x_i^{(I)}\phi_i^{(I)}/\sum_i x_i^{(N)}\phi_i^{(N)}$ of the isotropic phase relative to the coexisting nematic phase as a function of the composition of the isotropic $x_{iso} = x_2^{(I)}$. The filled circles indicate the inversion point of equal mass density. Ratios larger than unity correspond to the inverted state where the isotropic phase is denser than the coexisting nematic.

with the fact that the wavelength of the fastest growing mode should be larger than the critical wavelength. The latter is given by $2\pi(\gamma/\Delta\rho g)^{1/2}$, with γ being the interfacial tension, $\Delta\rho$ the density difference, and g the gravitational acceleration.[41] Guided by the work on sterically stabilized systems, the interfacial tension is estimated to be of the order $\gamma = 10^{-7}-10^{-8}$ N/m. This is in line with theoretical predictions for the interfacial tension of charged platelets based on the approximate Zwanzig model.[29] If we further estimate a density difference $\Delta\rho$ of about 0.1%, the critical wavelength is found to be less than 1 mm.

The fact that the formation of a columnar phase is not impeded by the considerable size polydispersity (particularly in the particle diameter) stands in contrast with the earlier studied sterically stabilized gibbsite system with similar polydispersity, where density inversion was observed, but no columnar phase could be found, even at very high particle concentrations.[21] A possible explanation could lie in the electric double layers surrounding the platelets. Due to electrostatic screening, both the plate diameter and thickness attain an effective value which is roughly equivalent to the bare value plus the Debye screening length. Consequently, the *effective* aspect ratio the platelets "feel" in solution is larger than the bare one, which may facilitate the formation of the columnar phase.

A remarkable feature of the theoretical phase diagram is that a demixing of the columnar phase is predicted if the overall concentration exceeds a certain value. At sufficiently high pressures, the columnar phase phase separates into an essentially pure fraction C_1 of thin platelets ($x_2 \sim 0$), and a bidisperse fraction C_2, both with a different overall packing fraction and associated intercolumnar spacing. The C_1 branch of the binodal is located on the vertical axis and meets the other branch at a critical point located at $x_2 \sim 0$. A detailed inspection of the free energy reveals that the same demixing scenario occurs at smaller thickness ratios with the critical pressure increasing rapidly for smaller ratios. If the thickness ratio is increased, the critical pressure shifts to lower values until the C_1-C_2 region eventually meets the N−C region at a triple pressure. At this point, a $N-C_1-C_2$ triple equilibrium occurs which is seen to span a wide composition range (see Figure 6). The coexistence of two columnar phases could not be realized experimentally presumably because the demixing process is suppressed by the glassy dynamics prevalent at these high particle concentrations.

VII. Conclusions

In this paper, we have explored the rich phase behavior of suspensions of charged platelets with a bimodal distribution in the aspect ratio with a combined experimental and theoretical effort. The isotropic−nematic phase separation is found to be accompanied by a large degree of shape fractionation, with the thick species strongly accumulating in the isotropic phase. The fractionation effect has a significant influence on the relative mass densities of the coexisting isotropic and nematic phases and leads to a *density inversion* where the top and bottom coexisting phases are seen to switch in a test tube as the overall plate concentration is gradually increased. Moreover, a distinct three-phase equilibrium involving an isotropic, nematic, and columnar phase is observed. We propose a simple, tractable theory based on the Onsager−Parsons free energy combined with a simple cell approach for the columnar state. By mapping the polydisperse, bimodal distribution onto a simple binary mixture of hard platelets of different thickness but common diameter, phase diagrams can be determined for various thickness ratios which bear out the fractionation scenario, density inversion, and triphasic equilibrium, in agreement with the experimental observations. At high pressures (which would correspond to concentrated samples), the theoretical phase diagram features an additional demixing of the mixture which gives rise to a coexistence between two columnar phases with distinctly different compositions and structures. For the larger thickness ratios, a triphasic nematic−columnar−columnar equilibrium is predicted. Experimentally, the high concentration regime is characterized by a dynamically arrested, metastable glassy state with local columnar order.

Acknowledgment. A.A.V. is grateful to the Royal Netherlands Academy of Arts and Sciences for financial support. Schlumberger Limited Company is acknowledged for funding the work of M.V. H.H.W. is financially supported by the Ramsay Memorial Fellowship Trust.

References and Notes

(1) Sanders, J. V.; Murray, M. J. *Nature* **1978**, *275*, 201.
(2) Sanders, J. V. *Philos. Mag. A* **1980**, *42*, 705.
(3) Hachisu, S.; Yoshimura, S. *Nature* **1980**, *283*, 188.
(4) Yoshimura, S.; Hachisu, S. *Prog. Colloid Polym. Sci.* **1983**, *68*, 59.
(5) Bartlett, P.; Ottewill, R. H.; Pusey, P. N. *Phys. Rev. Lett.* **1992**, *68*, 3801.
(6) Hunt, N.; Jardine, R.; Bartlett, P. *Phys. Rev. E* **2000**, *62*, 900.
(7) Schofield, A. B.; Pusey, P. N.; Radcliffe, P. *Phys. Rev. E* **2005**, *72*, 031407.
(8) Kajiwara, K.; Donkai, N.; Fujiyoshi, Y.; Inagaki, H. *Makromol. Chem.* **1986**, *187*, 2895.
(9) Sato, T.; Ikeda, N.; Itou, T.; Teramoto, A. *Polymer* **1989**, *30*, 311.
(10) Vroege, G. J.; Lekkerkerker, H. N. W. *J. Phys. Chem.* **1993**, *97*, 3601.
(11) Purdy, K. R.; Varga, S.; Galindo, A.; Jackson, G.; Fraden, S. *Phys. Rev. Lett.* **2005**, *94*, 057801.
(12) Varga, S.; Galindo, A.; Jackson, G. *Mol. Phys.* **2003**, *101*, 817.
(13) Brown, A. B. D.; Clarke, S. M.; Rennie, A. R. *Langmuir* **1998**, *14*, 3129.
(14) van der Kooij, F. M.; Lekkerkerker, H. N. W. *J. Phys. Chem. B* **1998**, *102*, 7829.
(15) van der Kooij, F. M.; Kassapidou, K.; Lekkerkerker, H. N. W. *Nature* **2000**, *406*, 868.
(16) Liu, S. Y.; Zhang, J.; Wang, N.; Liu, W. R.; Zhang, C. G.; Sun, D. J. *Chem. Mater.* **2003**, *15*, 3240.
(17) Fossum, J. O.; Gudding, E.; Fonseca, D. D. M.; Meheust, Y.; DiMasi, E.; Gog, T.; Venkataraman, C. *Energy* **2005**, *30*, 873.

(18) Michot, L. J.; Bihannic, I.; Maddi, S.; Funari, S. S.; Baravian, C.; Levitz, P.; Davidson, P. *Proc. Natl. Acad. Sci.* **2006**, *103*, 16101.
(19) Pusey, P. N. *J. Phys. (Paris)* **1987**, *48*, 709.
(20) Bates, M. A.; Frenkel, D. *J. Chem. Phys.* **1998**, *109*, 6193.
(21) van der Kooij, F. M.; van der Beek, D.; Lekkerkerker, H. N. W. *J. Phys. Chem. B* **2001**, *105*, 1696.
(22) Wensink, H. H.; Vroege, G. J.; Lekkerkerker, H. N. W. *J. Phys. Chem. B* **2001**, *105*, 10610.
(23) Bier, M.; Harnau, L.; Dietrich, S. *Phys. Rev. E* **2004**, *69*, 021506.
(24) Wensink, H. H. *Phys. Rev. Lett.* **2004**, *93*, 157801.
(25) Wierenga, A. M.; Lenstra, T. A. J.; Philipse, A. P. *Colloids Surf., A* **1998**, *134*, 359.
(26) van Bruggen, M. P. B.; Donker, M.; Lekkerkerker, H. N. W.; Hughes, T. L. *Colloids Surf., A* **1999**, *150*, 115.
(27) Lewis, D. J. *Proc. R. Soc. London, Ser. A* **1950**, *202*, 81.
(28) Rowan, D. G.; Hansen, J.-P.; Trizac, E. *Mol. Phys.* **2000**, *98*, 1369.
(29) Bier, M.; Harnau, L.; Dietrich, S. *J. Chem. Phys.* **2005**, *123*, 114906.
(30) Harnau, L.; Hansen, J.-P. *J. Chem. Phys.* **2002**, *116*, 9051.
(31) Onsager, L. *Ann. N.Y. Acad. Sci.* **1949**, *51*, 627.
(32) Parsons, J. D. *Phys. Rev. A* **1979**, *19*, 1225.
(33) Lee, S. D. *J. Chem. Phys.* **1987**, *87*, 4972.
(34) Lee, S. D. *J. Chem. Phys.* **1988**, *89*, 7036.
(35) Malijevsky, A.; Jackson, G.; Varga, S. *J. Chem. Phys.* **2008**, *129*, 144504.
(36) Odijk, T.; Lekkerkerker, H. N. W. *J. Phys. Chem.* **1985**, *89*, 2090.
(37) Odijk, T. *Liq. Cryst.* **1986**, *1*, 553.
(38) Vroege, G. J.; Lekkerkerker, H. N. W. *Rep. Prog. Phys.* **1992**, *55*, 1241.
(39) Lennard-Jones, J. E.; Devonshire, A. F. *Proc. R. Soc. London, Ser. A* **1937**, *163*, 53.
(40) Kirkwood, J. G. *J. Chem. Phys.* **1950**, *18*, 380.
(41) Chandrasekhar, S. *Hydrodynamic and hydromagnetic stability*; Dover Publications: 1961.
(42) The Debye screening length in a 10^{-2} M sodium chloride solution is 3 nm.
(43) The quantitative merits of the present theory can be tested against computer simulation results for a *monodisperse* system of platelets. This will be the subject of a forthcoming publication.

JP902858K